Angular and translational energy distributions of NO scattered from Pt(111)

1995 J. Phys.: Condens. Matter 7 5195

(http://iopscience.iop.org/0953-8984/7/27/007)

J. Phys.: Condens. Matter 7 (1995) 5195–5207. Printed in the UK

Angular and translational energy distributions of NO scattered from Pt(111)

A E Wiskerke and A W Kleyn

FOM-Instituut for Atomic and Molecular Physics, Kruislaan 407, 1098 SJ Amsterdam, The Netherlands

Received 14 November 1994, in final form 1 May 1995

Abstract. Time of flight spectra and final angle distributions are measured for NO scattered from Pt(111) at thermal up to hyperthermal initial kinetic energies (0.1–2.5 eV). The time of flight averaging, due to the finite experimental resolution, is deconvoluted with a simple parameter-free numerical procedure. The measured angular distributions show large widths (> 50°) for all initial energies. In addition, final translational distributions show a large spread with a mean translational energy of about half the initial energy.

1. Introduction

A surface scattering experiment is an excellent tool for investigating the dynamics of gas–surface interactions. The scattered distributions are determined by the shape of the gas–surface interaction potential and energy exchange. However, different types of gas–surface interaction may yield a similar outcome for a surface collision process. For instance, the width of an angular distribution may originate either from the lateral corrugation or from the thermal motion of the lattice. For collisions with initial kinetic energies E_i comparable with or less than $2kT_s$, the thermal motion of the surface (at temperature T_s) will be able to influence the distribution of scattered gas atoms or molecules. This is the region of thermal scattering. For increasing E_i or decreasing T_s, the transition from thermal scattering to so-called 'structure scattering' is reflected in the dependence of the final energy on the scattering angle (Goodman and Wachman 1976, Barker and Auerbach 1984). Thermal scattering will show higher final translational energies for subspecular scattering (the final angle Θ_f, measured from the surface normal, is smaller than the initial angle Θ_i) and lower energies for superspecular scattering ($\Theta_f > \Theta_i$). For flat surfaces this behaviour can be described by cube models, in which parallel momentum conservation is assumed (Yamamoto and Stickney 1970, Goodman and Wachman 1976). At hyperthermal energies when structure scattering prevails the angular and the final energy distributions directly reflect the shape of the scattering potential (Barker and Auerbach 1984, Kleyn and Horn 1991).

The presence of internal degrees of freedom for molecular collisions complicates the picture. Scattering of diatomic molecules from surfaces has been studied for several combinations of molecular projectiles and surfaces (see e.g. Barker and Auerbach 1984, Kleyn and Horn 1991, Kleyn 1994). Typically, the systems involve shallow wells (< 0.5 eV). In contrast, the NO–Pt(111) system, studied here, shows a deep chemisorption well with depth $\epsilon = 1$ eV (Campbell *et al* 1982, Serri *et al* 1983). In this study we focus our attention on the influence of this chemisorption well on the scattering dynamics. Earlier

0953-8984/95/275195+13$19.50

investigations of scattering of NO from Pt(111) have been performed for initial energies up to 0.25 eV (see e.g. Campbell *et al* 1982, Guthrie *et al* 1982, Serri *et al* 1982, Jacobs *et al* 1989, Kuipers *et al* 1989a, b, c, Tenner *et al* 1991). In this regime trapping–desorption is the predominant process. By increasing the initial kinetic energy to 2.5 eV, we are scanning from the trapping-dominated regime to the regime where mostly direct inelastic scattering occurs.

For NO molecules scattered from Pt(111) Jacobs and Zare have proposed three important processes: direct inelastic scattering, trapping–desorption and indirect inelastic scattering (Jacobs and Zare 1989). At the lowest initial kinetic energy (E_i), gas–surface interactions are dominated by trapping, possibly followed by desorption, depending on the surface temperature. Roughly speaking, trapping will be prevalent when $E_i < \epsilon$ (Trilling and Hurkmans 1976, Barker and Auerbach 1984). For NO–Pt(111) at $T_s = 673$ K, desorption will take place within 1 μs (Serri *et al* 1983). When $E_i \ll \epsilon$, trapping in the well is unlikely: direct scattering occurs, since the molecule cannot lose enough energy. For $E_i \approx \epsilon$, the dynamics may be more complicated and trapping can occur. In addition, so-called indirect inelastic scattering can occur, which is an intermediate between direct scattering and trapping–desorption. In this case, molecules will neither equilibrate to the surface nor show any sharp direct features, due to a kind of scrambling during the collision (Polanyi and Wolf 1985, Jacobs and Zare 1989). Such scrambling can occur when energy is temporarily stored as rotational energy which, if it is transferred to translational energy in a subsequent collision with the surface, makes escape from the well possible.

Direct scattering events represent the most simple trajectories probing the interaction potential. Final state distributions of directly scattered molecules give direct information on the processes involved. Recent measurements of rotational excitation have shown rainbow scattering for superspecular directions, indicating direct scattering despite the presence of a chemisorption well of 1 eV (Wiskerke *et al* 1993a, b, 1995).

At low energies, the greater proportion of the impinging molecules will stick to the surface in the case of NO–Pt(111). Brown and Luntz have measured an initial sticking probability S_0 of 0.9 for initial energies below 0.2 eV (Brown and Luntz 1993). Because of the large mass mismatch of NO and Pt, S_0 might be expected to drop quickly when E_i exceeds ϵ. However, the range of energies over which S_0 changes only gradually is large ($S_0 = 0.5$ at 1.6 eV), in contrast to what is observed for atom–surface interactions, such as K–W(110) (Hurkmans *et al* 1976) and Ar–Pt(111) (Mullins *et al* 1989, Rettner *et al* 1990, Head-Gordon *et al* 1991). The difference can be attributed to rotational excitation, which can provide a very efficient additional sticking mechanism (Harris and Luntz 1989). Since both the initial energy and the energy gained while the molecule is traversing the chemisorption well are available for rotational excitation, the amount of rotational excitation can be so large that insufficient translational energy is left for the molecule to escape. This mechanism has been shown to be active for NO adsorption at Ag(111) and is called rotationally mediated adsorption (Kuipers *et al* 1989a, b, c).

In the present study, the angular and translational energy distributions of the scattered NO molecules are measured as the kinetic energy increases from $E_i < \epsilon$ to $E_i > \epsilon$. In this way we intend to probe the gas–surface potential by scattering experiments that are not dominated by trapping in the deep chemisorption well. The energy transfer and the shape of the angular distributions provide information about the entire interaction potential.

Section 2 briefly addresses the measuring procedures and the specifics of our molecular beam machine. Special attention is given to the various ways of extracting the final translational energy flux distributions of scattered NO molecules from the observed time of flight (TOF) distributions. Section 3 contains the resulting angular and translational energy

flux distributions of scattered NO molecules impinging at the Pt(111) surface with an initial kinetic energy from 0.1 to 2.2 eV. Both the angular and the translational energy distributions turn out to be broad. The resulting average final energy and width of the angular distribution are compared to those observed for other cases of gas–surface scattering. The results are discussed in section 4. Section 5 reports the main findings of this study. The deconvolution procedure is described in an appendix.

2. Experimental details

The molecular beam apparatus has been described before by Spruit *et al* (1987). A molecular beam is generated by a supersonic expansion from a heatable nozzle. The quartz nozzle can be heated up to 1000 K. In order to cover a wide range of initial energies, mixtures of 2% NO in H_2, 2% NO in He and 5% NO in Ne are used. The highest initial energy that can be achieved is 2.5 eV for the heated nozzle and the NO–H_2 mixture. The rotational distributions of the initial beam are very cold. State selective measurements show a very low rotational temperature. Instead of a pure NO beam, a mixture of 5% NO in Ne is used to prevent cluster formation of NO molecules at low initial energies.

The crystal is cleaned by sputtering with 500 eV Ar^+ ions at a temperature of 900 K. In keeping with earlier studies (Verheij *et al* 1990), no subsequent annealing was necessary. To remove carbon from the surface, we dose with a background pressure of 10^{-5} Pa O_2. Oxygen that after this treatment remains on the surface is reduced with an H_2 background. During this cycle, we use He scattering to monitor the quality of the surface. The quality of the crystal is checked with He scattering and low-energy electron diffraction (LEED). The misalignment of the surface with the (111) crystal plane is less than 0.1°, as determined by Von Laue x-ray diffraction. NO does dissociate at steps on the Pt(111) face, leaving a small amount of atomic oxygen on the surface (Campbell *et al* 1982). During our measurements, H_2 is let into the chamber at a pressure of 10^{-6} Pa to remove the atomic oxygen. During measurements with NO–He mixtures, He scattering is used to monitor the cleanness of the crystal while the NO beam is on. These experiments showed that an H_2 pressure of 10^{-7} Pa is already sufficient to remove the atomic oxygen. Typically, after a three-hour scan the height of the specular He peak is 90% of the height before the scan.

In order to measure energy distributions, a TOF scheme with a rotating disc chopper is used. It produces pulses 15 μs wide, with an interval of 2 ms. Scattered molecules are ionized by electron impact, mass selected by means of a quadrupole mass spectrometer and detected by a channeltron in pulse counting mode. TOF spectra are recorded with a multichannel scaler with 2 μs resolution.

There are several factors determining the energy resolution of the experiment. By way of illustration, we decided to evaluate the energy resolution of the experimental set-up for measurements with an initial energy of 2.2 eV (NO velocity of 3760 m s^{-1}). For the incoming beam the pulse duration of 15 μs wide is substantial compared to the total flight time, which is 86 μs over the flight path of 322 mm from chopper to detector. Due to the spread in beam velocity, the pulse arriving at the surface will show an even larger width and the flight time after the collision is 47 μs over a flight path of only 175 mm to the detector. The widths of the pulses will cause the recorded TOF spectra to show slower transients.

The observed TOF spectra are the result of the convolution over the chopper function, initial speed distribution and final speed distribution. In order to find the final speed distribution, the measured TOF spectrum should be deconvoluted for the influence of the finite chopper pulse and the initial speed distribution. The convolution of the

chopper function and the initial speed distribution can be measured accurately. Up to now the deconvolution has been performed by means of fitting procedures assuming specific functional forms for the final TOF distributions. In many cases a shifted Maxwell–Boltzmann distribution has turned out to be a reasonable guess for the final TOF distributions. In the case of NO–Pt(111), however, the data deviate from such a distribution, as will be shown in this article. In addition, at high surface temperatures, trapping–desorption will take place within 1 ms and will be visible in the distribution, which is trailing the sharp direct inelastic peak. A reasonable fit can be obtained by the use of a double Maxwell–Boltzmann distribution consisting of a non-shifted and a shifted distribution:

$$F(v) = C_1 v^3 \, \mathrm{e}^{-((v-v_b)/v_{\alpha_1})^2} + C_2 v^3 \, \mathrm{e}^{-(v/v_{\alpha_2})^2} \tag{1}$$

where F is the scattered flux, v is the velocity and C_1, C_2, v_b, v_{α_1} and v_{α_2} are fitting parameters (Hurst *et al* 1983, Spruit *et al* 1989, Raukema *et al* 1995).

In this article we choose to present the data as energy distributions obtained by a TOF density to energy flux transformation. This means that we show raw or deconvoluted data, multiplied by $(l/t)^2$ and plotted against the energy found by means of the following equation:

$$E = \frac{1}{2} m \left(\frac{l}{t} \right)^2 \tag{2}$$

where t equals the time between the arrival of the beam pulse on the surface and the time of detection, and l equals the flight path between surface and detector. The flux distribution obtained for $E_i = 2.2$ eV, $\Theta_i = \Theta_f = 40°$ is plotted as a function of final energy in figure 1. The result of fitting the distribution with equation (1) is also shown in this figure. The appearance of a thermal (non-shifted) Boltzmann distribution with a temperature of 4014 K is very unphysical for trapping–desorption in this system, and is most likely due to the inadequacy of a shifted Maxwell–Boltzmann distribution for fitting the present results. Therefore, we will analyse the data in another way. This makes it possible to extract the translational energy flux distribution of scattered NO molecules without having to invoke simple trial functions, such as (modified) Boltzmann distributions. The deconvolution method is described in detail in the appendix. If the deconvolution is omitted, the final energy distributions are changed with respect to the fitted distributions. As can be seen in figure 1, this crude and direct method of extracting a final energy distribution from a TOF measurement shows slightly different results. The deviations from the distributions obtained from deconvoluted data are surprisingly small.

3. Results

The eight panels of figure 2 show the main results of the experiments. The distributions of scattered NO molecules are displayed as contour plots as a function of the final scattering angle Θ_f and the final translational energy E_f of the scattered NO flux. Θ_f and the angle of incidence Θ_i are defined with respect to the surface normal. The sticking probability S_0 is given in all panels (Brown and Luntz 1993).

The contours show very broad distributions in all panels. The maximum of the distribution is found near $E_f \approx 0.5E_i$ and $\Theta_f \approx \Theta_i + 10°$. The energy distributions

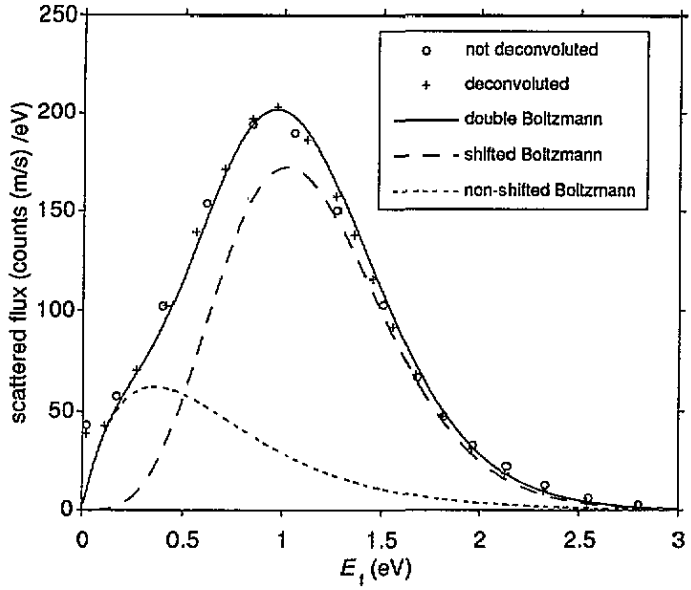

Figure 1. Final translational energy distribution for $E_i = 2.2$ eV, $\Theta_i = 40°$ and $\Theta_f = 40°$. The full line is the distribution fitted in the time domain to the data with the double Boltzmann function (equation (1)). The dashed line is the contribution of the shifted Boltzmann distribution, and the dotted line represents the non-shifted Boltzmann distribution. Data points directly converted using equation (2) are depicted by the circles. The plus signs represent the same data, deconvoluted by means of the iteration scheme in figure 2. Parameters for the fitted distribution defined by equation (1) are $v_b = 2329$ m s^{-1}, $v_{\alpha_1} = 766$ m s^{-1} ($T = 1059$ K), $v_{\alpha_2} = 1519$ m s^{-1} ($T = 4015$ K).

extend from zero to more than E_i. For $E_f = 0.1$ eV, final energies up to $2E_i$ are found for $\Theta_f = 20°$. Only at the most superspecular scattering angles does the translational energy distribution narrow down to $E_f = 0.5E_i$. The broad distributions might be anticipated for low-energy scattering.

Although S_0 is not sensitive to Θ_i, the subspecular scattering distribution is found to be dependent on Θ_i. The comparison of the panels b and h of figure 2, with $E_i = 2.2$ eV, $\Theta_i = 60°$ and with respectively $T_s = 474$ K or 673 K, shows the contribution of trapping–desorption at $T_s = 673$ K. This observation supports the assumption that (in)direct inelastic scattering is the source of all other data reported in this study.

Figure 3 displays the integrated flux distributions for various E_i normalized (see figure caption) on the incident beam intensity together with $\langle E_f \rangle / E_i$ as a function of Θ_f. These data were evaluated by means of the successive approximation deconvolution scheme presented in the appendix. The most dominant features of the measurements are again the broad angular width and a broad final energy distribution. The angular distributions as well as the E_f/E_i distributions are only weakly dependent on the initial energy. The increase observed in the relative intensities of the scattered signal roughly matches the decrease observed in S_0.

The scattered distributions show no evidence for parallel momentum conservation. This becomes very clear if the final energies are compared to the lines computed for parallel momentum conservation in figure 3. Especially for $\Theta_i = 60°$, the mean final energy shows an opposite behaviour: the final energy increases with final angle, which is the case for

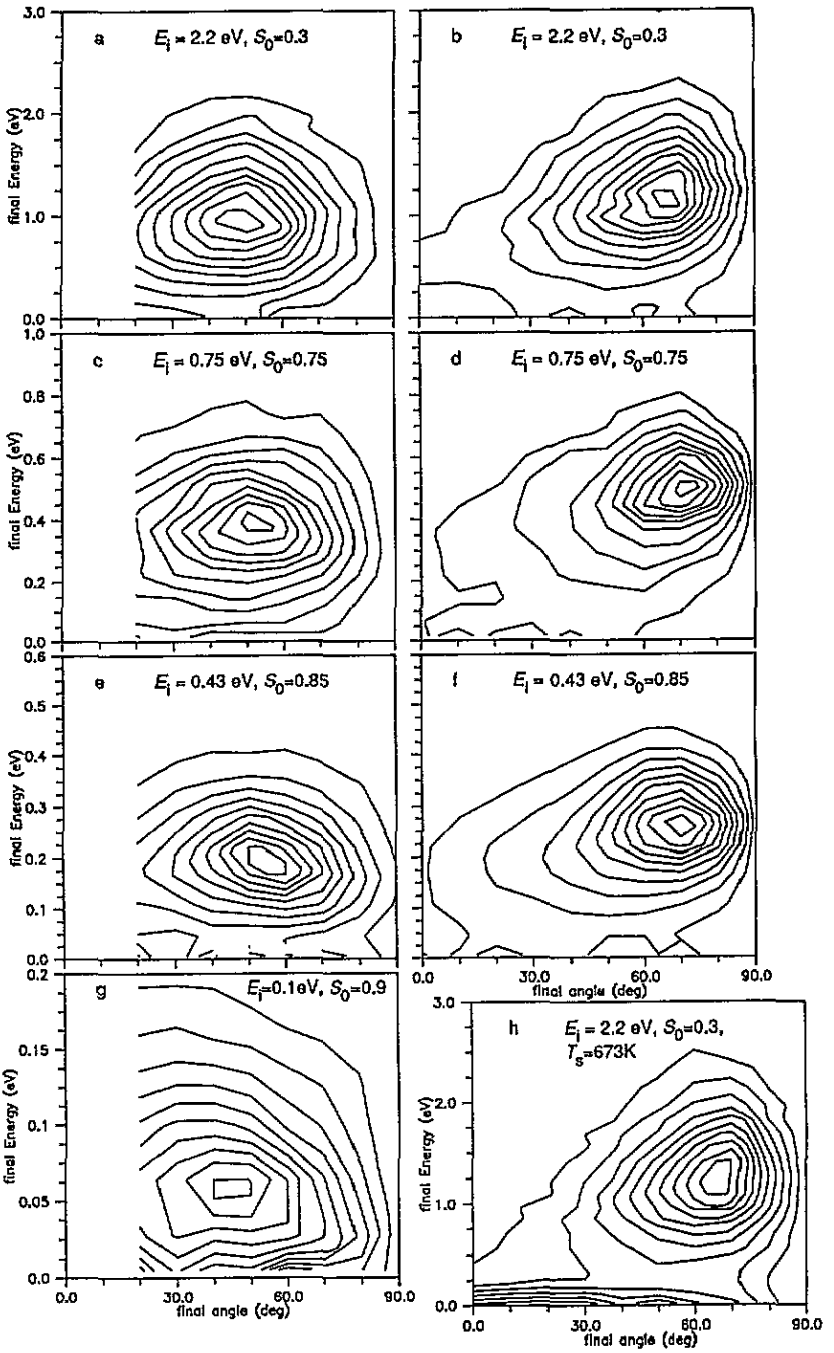

Figure 2. Contour plots of scattered distributions. Panels on the left depict results for $\Theta_i = 40°$; panels on the right depict results for $\Theta_i = 60°$. Plotted are the scattered intensities against final angle (horizontally) and final energy (vertically). The incident energy E_i and the sticking probability S_0 are indicated in all panels. The contour lines show a single maximum to the right of the specular angle. The highest contour level corresponds to 95% of the peak height. The lines are equally spaced and plotted at 85%, 75% etc. The panels a–g are taken with T_s = 473 K; panel h shows a distribution taken at T_s = 673 K. Here, trapping–desorption is visible as a separate peak at low energies.

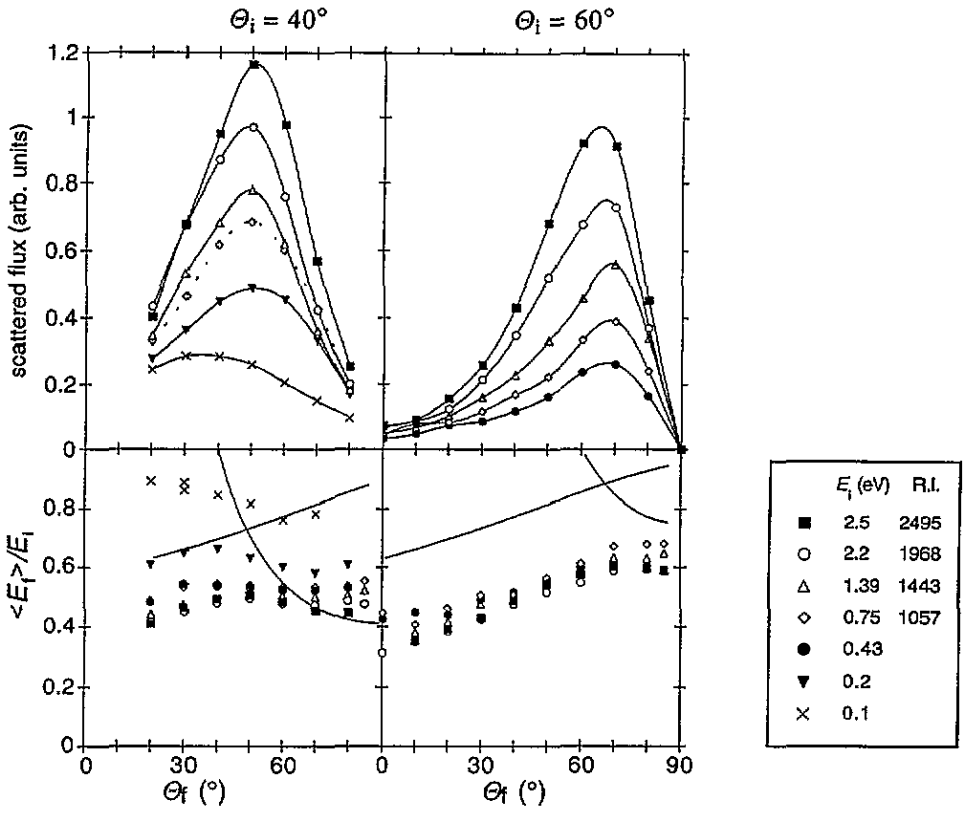

Figure 3. Experimental results for scattering of NO from Pt(111). Plotted are $\langle E_f \rangle / E_i$ (lower panels) and the final flux distributions (upper panels) as a function of Θ_f. The lines drawn in the upper panels through the symbols serve to guide the eye. In the lower panels, the 'straight' lines show the dependence of E_f/E_i on Θ_f computed for a binary elastic NO–Pt atom collision. The curved lines show the same dependence, in this case computed for parallel momentum conservation. The relative intensities RI for $\Theta_i = 60°$ have been obtained by normalization to the incident flux, for $E_i \geqslant 0.75$ eV. For $E_i < 0.75$ eV, scaling is arbitrary.

a binary collision as well. Compared to a binary collision model, which assumes gas-phase-like scattering without rotational excitation, the trend of increasing final energy with increasing final angle is reproduced. The amount of energy lost in the binary collision, however, is much less than observed in NO–Pt(111). The extra energy lost for NO–Pt(111) scattering may be attributed to rotational excitation and to collisions involving more than one surface atom.

The shape of the final energy distribution of NO–Pt(111) appears to be very different from distributions we measured for other systems, like Ne, Ar and O_2 scattered from Pt(111), as can be seen in figure 4. Molecular systems having weak attractive interactions, like NO–Ag(111) (Kuipers *et al* 1987), and even systems where atomic chemisorption can take place, like O_2 from Pt(111) (Wiskerke *et al* 1992), show final energy distributions that are comparable to the distributions for Ne–Pt(111) and Ar–Pt(111). NO–Pt(111) shows much broader energy distributions, due to the strong attractive potential.

The angular widths of NO–Pt(111) are very large compared to any other system. This is illustrated in figure 5. For $\Theta_i = 40°$, the angular widths are about 40° for initial energies

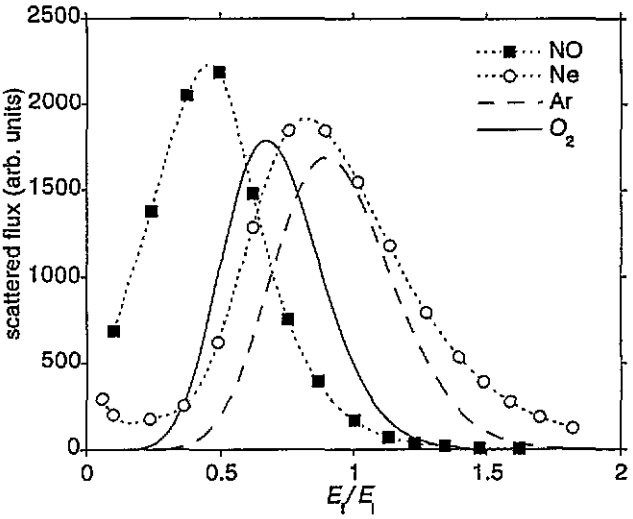

Molecule	E_i (eV)	$\Theta_i = \Theta_f$ (°)	T_s (K)	$\frac{1}{2}kT_s/E_i$
NO	0.43	40	473	0.047
Ne	0.14	40	473	0.145
Ar	0.25	45	900	0.155
O_2	0.46	40	373	0.035

Figure 4. Final translational energy distributions for NO, Ne, Ar and O_2 scattered from Pt(111). *The conditions for the measurements are listed in the table below. The dotted lines through the* symbols are drawn to guide the eye.

above 0.2 eV and decrease very gradually when the initial energy increases. Energies lower than 0.2 eV result in even greater widths.

4. Discussion

The width of an angular distribution of (hyper)thermal molecule–surface scattering exhibits a characteristic behaviour as can be seen for several systems in figure 5: the distribution is very broad at thermal energies, narrows for energies up to 1 eV and broadens again for higher energies. This has been seen clearly in very recent classical trajectory calculations for Ar scattering from Ag(111) (Lahaye *et al* 1995). The broadening at low energies is due to energy transfer from the lattice to the gas particle, as predicted by cube models, due to thermal roughening of the surface and to a smaller extent due to refraction effects in the attractive well of the potential (Harris *et al* 1982). Energy transfer is important irrespective of the detailed shape of the potential as long as the beam energy is on the order of the thermal energy of the surface. Indeed, we observe in the energy transfer measurements at $\Theta_i = 40°$ and $E_i = 0.1$ eV that the final energy is fairly high and in the vicinity of the hard cube line, computed for parallel momentum conservation. The other sources of broadening, thermal roughening and refraction, cannot be isolated in the experiments at 0.1 eV, especially because of the high trapping probability.

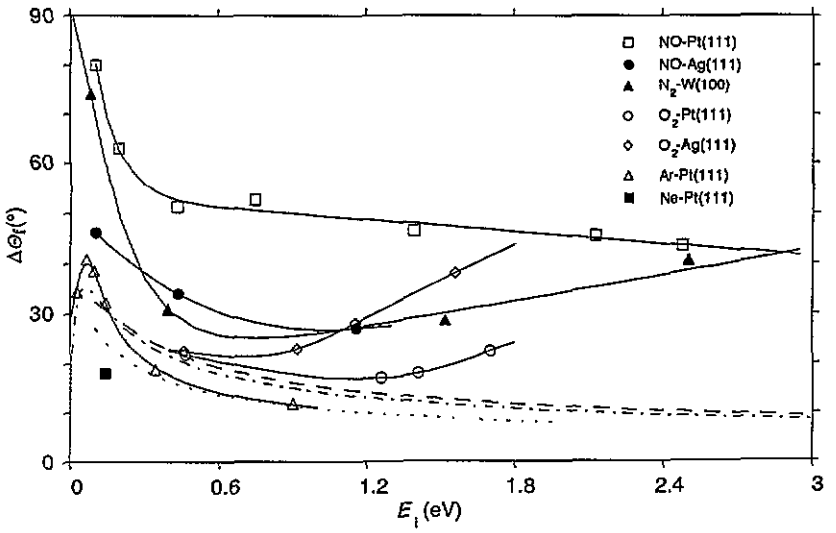

System	Θ_i (°)	T_s(K)	M_g/M_s	Reference
NO-Pt(111)	40	473	0.154	this study
NO-Ag(111)	45	573	0.278	(Kuipers et al. 1987)
N_2-W(100)	45	800	0.152	(Rettner et al. 1990)
O_2-Pt(111)	40	400	0.164	(Wiskerke et al. 1992)
O_2-Ag(111)	38	573	0.297	(Spruit et al. 1989)
Ar-Pt(111)	45	500	0.205	(Hurst et al. 1983)
Ne-Pt(111)	40	473	0.103	this study

Figure 5. Angular widths for various systems. The dotted, dashed and dash–dotted lines are results from cube calculations. The dotted line represents calculations with a mass ratio of $\frac{32}{195}$ and $T_s = 400$ K (O_2–Pt), the dashed line with a mass ratio of $\frac{32}{150}$ and $T_s = 600$ K (O_2–Ag), and the dash-dotted line represents calculations with a mass ratio of $\frac{40}{195}$ and $T_s = 500$ K (Ar–Pt). The table below gives the experimental conditions and the reference for each system.

At higher energies the effect of the thermal motion is reduced and the angular width is determined by the corrugation of the surface, which for most systems increases with energy. In the calculations of Ar on Ag(111) this increase is dramatic. For NO scattering from Pt the molecules are accelerated in a well of depth 1 eV. For energies up to at least 1 eV the corrugation felt by the molecules will be mainly due to the acceleration in the well. Further broadening of the angular distributions may occur due to refraction in the well along the exiting trajectory. One would expect the angular width to be comparable to what is seen for other systems at energies of about an eV higher. Figure 5 shows that the NO–Pt width is indeed approaching the width for some other systems around $E_i = 2$ eV. Interestingly, for the O_2–Ag(111) system the sharp increase of the width with energy has been attributed to the fact that the molecules sample the corrugated repulsive wall of the chemisorption potential (Raukema *et al* 1995). Two repulsive walls can be probed in those

experiments: the 'outer' wall of the physisorption potential at low energies and the 'inner' one of the chemisorption potential when $E_i > 1$ eV, which is not accessible near thermal energies because of a barrier. In the case of NO–Pt(111) such a barrier does not exist and the chemisorption potential is probed at all energies. The effect of acceleration in the well and refraction should decrease with collision energy. Hence one would expect the width to decrease with energy. On the other hand, the static corrugation increases with energy as seen for many systems. Apparently the two effects cancel for NO–Pt and the width remains large over the entire energy range: the well masks the change in scattering mechanism, which is visible for other systems.

A similar cancellation is apparent in the energy transfer curves in figure 3. Increasing E_i above 0.1 eV leads to a rapid convergence of the energy transfer curves. The curves remain essentially below the energy transfer computed for a binary collision, which indicates that multiple collisions and/or substantial rotational excitation occur. The latter has indeed been observed and almost accounts for the 'missing' translational energy (Wiskerke *et al* 1995). Similar energy transfer curves are seen for e.g. Xe–Pt(111) and O_2–Ag(111) or O_2–Ag(110) (Barker and Rettner 1992, Barker *et al* 1991, Barker and Rettner 1994, Raukema *et al* 1995). In the latter case the energy transfer curves are close to the binary collision line.

In the discussion so far the effect of trapping in the chemisorption well has been ignored. If trapping were to give rise to selection effects in scattering, this assumption would be incorrect. Elsewhere we have demonstrated the presence of such selection effects. A rotational rainbow is clearly visible for $\Theta_f = 70°$ and 0.3 eV $< E_i <$ 1.0 eV. It has been suggested to be due to the presence of a shallow well when the O end of the NO molecule approaches the Pt(111) surface at certain sites (Wiskerke *et al* 1993). For those orientations and sites, the NO–Pt(111) interaction is presumably quite similar to the NO–Ag(111) interaction. This is confirmed by the fact that the high-J parts of the rotational excitation are similar at $E_i \approx 0.3$ eV (Geuzebroek *et al* 1991, Wiskerke *et al* 1993). The overall effect is very small on the entire angular distribution and energy transfer curve. Therefore, in the discussion of the overall dynamics subtleties like rotational rainbows play a minor role.

The data suggest that a large amount of averaging over some very complex interactions takes place and determines the final insensitivity of the angular distributions and energy transfer to the incident energy. To investigate this further we have performed a statistical analysis of NO–Pt(111) scattering (Taatjes *et al* 1995). In our models we assume that complete randomization occurs between the incident (normal) energy, rotational energy and thermal energy of a limited number of surface oscillators. The models describe the measured angular distributions and rotational state distributions outside the regime of rotational rainbow scattering quite well. The model cannot properly describe the energy transfer to the lattice and rotational excitation simultaneously. This suggests that energy transfer to rotation and to the lattice cannot be described entirely statistically. Nevertheless, the model suggests that very efficient transfer of energy between the various degrees of freedom occurs. A physical explanation for this can be found in the frequent occurrence of chattering and multiple hops of the molecule at the surface. The deep well is responsible for these events. From the present experimental results we can conclude that very efficient energy transfer between all degrees of freedom of the system occurs from thermal energies up to at least 2.5 eV. This randomization also explains why there is no distinct change in the angular and energy distributions when the sticking probability starts to decrease. At this energy the impulsive limit of surface scattering, direct reflection of a hard anisotropic

shell from (an array of) individual atoms has not yet been reached (VanSlooten *et al* 1992, VanSlooten and Kleyn 1993).

5. Conclusions

NO scattered from Pt(111) shows very broad angular and final translational energy distributions for direct scattering. The distributions are only weakly dependent on the initial energy at $E_i > 0.2$ eV. At lower initial energies, the distributions are even broader, which expresses the increasing importance of the surface temperature. Apparently, the deep well enhances energy transfer and increases the width of the energy distributions. This broadening may be caused by indirect scattering, in which case the initial energy is scrambled, presumably due to multiple collisions. The well will also increase the static corrugation of the repulsive potential. This, in turn, will lead to wide angular distributions.

Acknowledgments

We thank Steven Stolte for the stimulating discussions and his valuable comments on the manuscript. The help of Brian Hayden in the early stages of the experiments is highly appreciated. This work is part of the research program of the Stichting voor Fundamenteel Onderzoek der Materie (Foundation for Fundamental Research on Matter) and was made possible by financial support from the Nederlandse Organisatie voor Wetenschappelijk Onderzoek (Netherlands Organization for Scientific Research).

Appendix

Our newly developed deconvolution procedure can be described as follows. The measured data of the time of flight distribution, as collected by the $n = 1024$ channels of the multichannel scalar, can be represented as a histogram, the g array. The measured peak of the TOF distribution of the direct beam is transformed into a distribution, which describes the time profile of the beam pulse as it hits the surface. The time profile is collected in a n-channel histogram c. Most of its elements are zero, because the beam pulse is very sharp in the time domain all elements of which are zero. The array c is normalized as $\sum c_i = 1$. The array f (n channels wide) represents the deconvoluted TOF distribution; it can be found by solving the following equation:

$$g_i = \sum_{\hat{i}}^{i} c_{\hat{i}} \cdot f_{(i-\hat{i}) \bmod n}. \tag{A1}$$

Since the measured TOF distribution is periodic with a period of n, the mod function in the index of the equation can be used. A general problem with deconvolution is the noise that is present in the signal. The solution of equation (A1) provides a function in which measured fluctuations are amplified. When g rises faster than the rising flank of the chopper function or when the signal decays faster than the decaying flank of the chopper function, f has to show these rapid fluctuations. We have chosen to solve this problem by using a successive approximation scheme. The algorithm we used (presented in figure A1) generates a smooth function giving a convoluted signal that falls within the noise of the measured

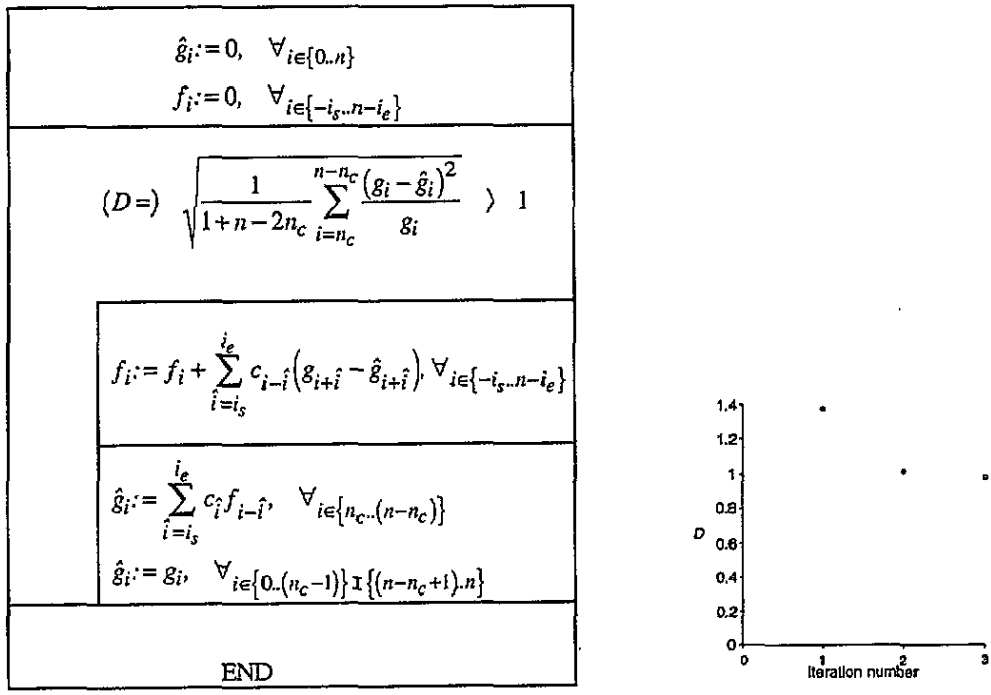

Figure A1. A schematic (Nassi–Shneidermann) diagram of the algorithm used for deconvoluting TOF data. i_s: number of the first channel of the chopper function; i_e: number of the last channel of the chopper function; n: number of channels in the measurement; $n_c = i_e - i_s + 1$. This algorithm contains one loop. It stops when the control becomes less than unity. The graph depicts the evolution of the control variable D.

distributions. The cross-correlation of g and c is a first estimate for f. Subsequently, in each successive approximation step the cross-correlation of the deviation of g found by the convolution of f and the measured value of g is taken to correct the actual f array. This procedure suppresses fluctuations in f that appear to be faster than the pulse shape of c. Eventually, this algorithm will solve equation (A1) exactly. In that case the control variable D approaches zero, illustrating the convergence of the procedure (Goldberg 1979). The exact solution of equation (A1), however, shows rapid undulations, caused by the counting statistics in the measured function g. The deviations from the expectation value of a measured quantity g in the case of counting statistics have to fulfil the condition

$$\left\langle \frac{(g-\langle g\rangle)^2}{\langle g\rangle} \right\rangle = 1. \tag{A2}$$

The control variable D in figure A1 is based on this relation. If this variable is less than unity, we are overinterpreting the data. The initial beam for the measurement shown in figure 1 has a high energy (is very fast) and, accordingly, the velocity dispersion in the beam hardly contributes to the pulse width impinging on the crystal. Therefore, deconvolution of the chopper function is sufficient. The pulse arriving at the crystal may be spread in time, due to the energy spread in the beam. In that case an estimate for the pulse shape of the beam impinging on the crystal can be used.

References

Barker J A and Auerbach D J 1984 *Surf. Sci. Rep.* **4** 1
Barker J A and Rettner C T 1992 *J. Chem. Phys.* **97** 5844
—— 1994 *J. Chem. Phys.* **101** 9202
Barker J A, Rettner C T and Bethune D S 1992 *Chem. Phys. Lett.* **188** 471
Brown J K and Luntz A C 1993 *Chem. Phys. Lett.* **204** 451
Campbell C T, Ertl G and Segner J 1982 *Surf. Sci.* **115** 309
Geuzebroek F H, Wiskerke A E, Tenner M G, Kleyn A W, Stolte S and Namiki A 1991 *J. Phys. Chem.* **95** 8409
Goldberg M A 1979 *Solution Methods for Integral Equations. Theory and Applications* ed M A Goldberg (New York: Plenum) p 1
Goodman F O and Wachman H Y 1976 *Dynamics of Gas–Surface Scattering* (New York: Academic)
Guthrie W L, Lin T-H, Ceyer S T and Somorjai G A 1982 *J. Chem. Phys.* **76** 6398
Harris J, Liebsch A, Comsa G, Mechtersheimer G, Poelsema B and Tomoda S 1982 *Surf. Sci.* **118** 279
Harris J and Luntz A C 1989 *J. Chem. Phys.* **91** 6421
Head-Gordon M, Rettner C T, Mullins C B, Auerbach D J and Tully J C 1991 *J. Chem. Phys.* **94** 1516
Hurkmans A, Overbosch E G and Los J 1976 *Surf. Sci.* **59** 488
Hurst J E, Wharton L, Janda K C and Auerbach D J 1983 *J. Chem. Phys.* **78** 1559
Jacobs D C, Kolasinski K W, Shane S F and Zare R N 1989 *J. Chem. Phys.* **91** 3182
Jacobs D C and Zare R N 1989 *J. Chem. Phys.* **91** 3196
Kleyn A W 1994 *Surf. Rev. Lett.* **1** 157
Kleyn A W and Horn T C M 1991 *Phys. Rep.* **199** 191
Kuipers E W, Tenner M G, Kleyn A W and Stolte S 1989a *Chem. Phys.* **138** 451
—— 1989b *Phys. Rev. Lett.* **62** 2152
—— 1989c *Surf. Sci.* **211/212** 819
Kuipers E W, Tenner M G, Spruit M E M and Kleyn A W 1987 *Surf. Sci.* **189/190** 669
Lahaye R J W E, Stolte S, Kleyn A W and Holloway S 1995 *Surf. Sci.* submitted
Mullins C B, Rettner C T, Auerbach D J and Weinberg W H 1989 *Chem. Phys. Lett.* **163** 111
Polanyi J C and Wolf R J 1985 *J. Chem. Phys.* **82** 1555
Raukema A, Dirksen R J and Kleyn A W 1995 *J. Chem. Phys.* submitted
Rettner C T, Mullins C B, Bethune D S, Auerbach D J, Schweizer E K and Weinberg W H 1990a *J. Vac. Sci. Technol.* A **8** 2699
Rettner C T, Schweizer E K and Stein H 1990b *J. Chem. Phys.* **93** 1442
Serri J A, Cardillo M J and Becker G E 1982 *J. Chem. Phys.* **77** 2175
Serri J A, Tully J C and Cardillo M J 1983 *J. Chem. Phys.* **79** 1530
Spruit M E M, Kuipers E W, Geuzebroek F H and Kleyn A W 1989a *Surf. Sci.* **215** 421
Spruit M E M, Kuipers E W, Tenner M G, Kimman J and Kleyn A W 1987 *J. Vac. Sci. Technol.* A **5** 496
Spruit M E M, VanDenHoek P J, Kuipers E W, Geuzebroek F H and Kleyn A W 1989 *Surf. Sci.* **214** 591
Taatjes C A, Wiskerke A E and Kleyn A W 1995 *J. Chem. Phys.* **102** 3848
Tenner M G, Kuipers E W, Kleyn A W and Stolte S 1991 *J. Chem. Phys.* **94** 5197
Trilling L and Hurkmans A 1976 *Surf. Sci.* **59** 361
VanSlooten U, Andersson D R, Kleyn A W and Gislason E A 1992 *Surf. Sci.* **274** 1
VanSlooten U and Kleyn A W 1993 *Chem. Phys.* **177** 509
Verheij L K, Hugenschmidt M B, Poelsema B and Comsa G 1990 *Chem. Phys. Lett.* **174** 449
Wiskerke A E, Geuzebroek F H, Kleyn A W and Hayden B E 1992 *Surf. Sci.* **272** 256
Wiskerke A E, Taatjes C A, Kleyn A W, Lahaye R J W E, Stolte S, Bronnikov D K and Hayden B E 1993a *Faraday Discuss.* **96** 297
—— 1993b *Chem. Phys. Lett.* **216** 93
—— 1995 *J. Chem. Phys.* **102** 3835
Yamamoto S and Stickney R E 1970 *J. Chem. Phys.* **53** 1594